Combined experimental/numerical investigation of directional moisture diffusion in glass/epoxy composites

Rocha, I. B.C.M.; Raijmaekers, S; van der Meer, F. P.; Nijssen, R. P.L.; Fischer, H. R.; Sluys, L. J.

DOI
10.1016/j.compscitech.2017.08.002

Publication date
2017

Document Version
Accepted author manuscript

Published in
Composites Science and Technology

Citation (APA)
Rocha, I. B. C. M., Raijmaekers, S., van der Meer, F. P., Nijssen, R. P. L., Fischer, H. R., & Sluys, L. J. (2017). Combined experimental/numerical investigation of directional moisture diffusion in glass/epoxy composites. *Composites Science and Technology*, *151*, 16-24. https://doi.org/10.1016/j.compscitech.2017.08.002

Combined experimental/numerical investigation of directional moisture diffusion in glass/epoxy composites

I. B. C. M. Rocha[1,2], S. Raijmaekers[1], F. P. van der Meer[2], R. P. L. Nijssen[1], H. R. Fischer[3], and L. J. Sluys[2]

[1]Knowledge Centre WMC, Kluisgat 5, 1771MV Wieringerwerf, The Netherlands

[2]Delft University of Technology, Faculty of Civil Engineering and Geosciences, P.O. Box 5048, 2600GA Delft, The Netherlands

[3]TNO Technical Sciences, De Rondom 1, 5612AP Eindhoven, The Netherlands

Abstract

A combined experimental and numerical investigation is conducted on the anisotropic water diffusion behaviour of unidirectional glass/epoxy composites. Experimental diffusivity values are obtained by immersing thin material slices for each of its planes of orthotropy extracted from a thick composite panel and interphase measurements are performed using thermal analysis. In order to elucidate the observed anisotropy, the diffusion process is modelled at the microscale using a representative volume element (RVE) of the material with random fibre distribution. Water concentration gradients are applied to the micromodel and a homogenisation procedure is used to retrieve the macroscopic diffusivity coefficients. The influence of the interphase around the fibres on the diffusion process is modelled by making the matrix diffusivity a function of the distance to the nearest fibre using a level set field. The models are used to fit the experimental data and test a number of hypotheses that may explain the observed anisotropy. The effect of fibres acting as barriers for water movement is found to partially explain the observed transverse diffusivity. However, a fit is only obtained by allowing faster diffusivity at the interphase. In the longitudinal direction, a fit can only be found by allowing for orthotropic interphase diffusivity.

Keywords: Water diffusion, Anisotropy, Fibre/matrix interphase, Homogenisation

1 Introduction

The influence of hygrothermal ageing, a combination of high temperatures and moisture ingression, on the mechanical behaviour of composite materials is an important design driver for structures such as

wind turbine rotor blades, which are required to withstand extreme service environments. Experimental characterisation of the hygrothermal ageing phenomenon remains a challenging research area, despite the already large body of literature on the subject. Many of the current knowledge gaps stem from the fact that hygrothermal ageing is a complex combination of physical and chemical phenomena that operate at different time and spatial scales [1]. Furthermore, the incurred degradation strongly depends on the material components involved [2] and on the exposure environment.

Over the past few years, a number of experimental studies on hygrothermal ageing has been performed with focus on elucidating the underlying microscopic degradation mechanisms, such as differential swelling, plasticization and interface debonding [3, 4, 5, 6], responsible for the impact of ageing on macroscopically measured material properties. Additionally, with the advent of novel numerical analysis techniques such as concurrent multiscale finite element analysis (FE^2) [7] and the development of advanced material models [8], such degradation mechanisms can be modelled and their nonlinear interactions can be captured across spatial scales.

However, since the ageing process is driven by water ingression, it is also important to understand the process of water diffusion across scales. For fibre reinforced polymers, the material microstructure brings complexity to the diffusion phenomenon since water molecules have to go around the fibres for diffusion in transverse direction [9], giving rise to orthotropic diffusion behaviour. Furthermore, chemical interaction between the epoxy and fibre sizing creates an interphase region around the fibres where water diffusivity can be different from the one in bulk resin regions [3].

In this work, a combined experimental and numerical approach was used to elucidate the water diffusion process in composite laminates, expanding upon early results published by the authors as a conference paper [10]. For the present contribution, new experimental interphase measurements are included, the numerical formulations are presented in greater detail, new calibration examples are presented and additional results and discussion are included. For the experimental part, a thick unidirectional glass/epoxy composite panel was manufactured and thin slices were cut along the three orthotropy planes of the material. The slices were immersed in demineralised water at 50°C and weighed at regular intervals. By fitting a unidimensional analytical solution of Fick's second law of diffusion to the experimentally obtained water uptake curves, the orthotropic diffusivity constants were retrieved. Using a combination of scanning thermal microscopy and local thermal analysis, the presence of an interphase was confirmed for the present composite system and its approximate thickness was measured.

The diffusivity coefficients were also numerically obtained through homogenisation of the microscopic diffusion behaviour. For this purpose, a three-dimensional Representative Volume Element (RVE) was subjected to water concentration gradients in each direction. By integrating the flux components in the microscopic volume, homogenised diffusivity values were obtained. In order to account for the impact of

the fibre/matrix interphase on the diffusion process, the resin diffusivity was made a function of the distance to the nearest fibre. A parametric study on the RVE size and mesh density was performed and the model was used to verify the validity of a number of hypotheses put forward in literature that may explain the observed anisotropy.

2 Experiments

2.1 Materials

The material system considered in the present study consists of the epoxy resin EPIKOTE 135/1366, manufactured by Momentive [11], with embedded unidirectional glass fibre fabrics (Saertex PPG 2002 2400tex [12]). For the resin preparation, the monomer and hardener were mixed in a 100:30 ratio and the resultant mixture was degassed in vacuum in order to minimise void content. Unidirectional glass fibre plies were stacked and infused through vacuum bagging in a heated flat mould.

In order to experimentally investigate the anisotropic diffusion behaviour through weight measurements, specimens must be devised in such a way that the water movement in a certain direction is promoted while diffusion in the other directions is minimised. This can be achieved by selectively sealing specimen edges [13] or by cutting thin material slices in each direction [9]. Here, the latter procedure was chosen and a thick laminate of 50 unidirectional (UD) plies (total thickness of 30 mm) was manufactured in order to obtain specimens with high width/thickness and length/thickness ratios for three different orientations.

Each UD fabric ply used in the manufacturing was mainly composed of fibres oriented at 0° (95% in weight) with stability rovings oriented at 90° accounting for 5% of their weight. In order to obtain a purely UD laminate, the stability rovings were manually removed prior to infusion. The panel was cured for 3 hours at 30°C and 5 hours at 50°C, with a subsequent post-curing period of 10 hours at 70°C. After curing, 30 x 30 mm^2 slices were cut from the panel along the three orthotropy planes of the material, as shown in Figure 1.

Three slices were cut in each direction using a water-cooled diamond saw and were grinded with a Labopol 30 polishing machine using progressively higher sanding grits ranging from 320 to 1200 until a thickness of 0.9 mm was reached, resulting in width/thickness and length/thickness ratios of approximately 30. The average thickness among the nine slices was 0.94±0.06 mm, while the average ratio was 31.9±2.3. Finally, the surfaces were polished using a suspension of diamond particles with average diameter of 1 μm. The final surfaces were inspected for defects using a Motic BA210 optical microscope, although the occurrence of microscopic failure events such as interface debonding during specimen preparation cannot be completely ruled out. Using three additional specimens, average values of fibre volume fraction of

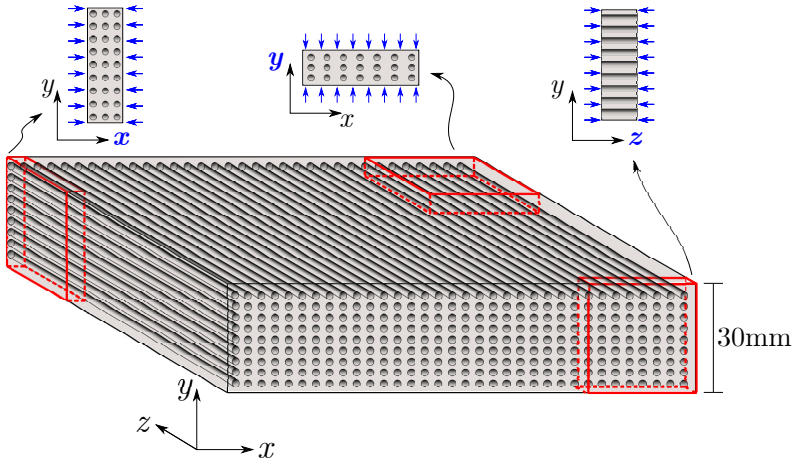

Figure 1: Material slices and preferred diffusion directions.

53.1±0.27% and void content of 0.85±0.21% were obtained through loss on ignition, according to the ISO 1172 standard.

2.2 Conditioning

In order to obtain accurate measurements of the maximum water uptake, the slices were first dried for approximately 200 h in a desiccator at 50°C, after which a stable weight was achieved. The choice of the reference state in diffusion experiments on polymer matrix composites can be a complex one, since additional ageing processes such as physical ageing and oxidation can occur during the initial drying phase. Due to changes in the polymer structure caused by these additional ageing mechanisms, the diffusivity and the maximum uptake may suffer both reversible and irreversible changes [14, 15]. In this work, oxidative reactions were avoided by applying vacuum to the desiccator during the drying process, while the short duration of the drying phase, enabled by the use of thin slices, helped to minimise the influence of physical ageing.

The slices were subsequently immersed in demineralised water kept at a temperature of 50±1.5°C. This immersion temperature was chosen in order to accelerate water uptake while keeping a safety margin of 20°C from the glass transition temperature (T_g) measured in saturated resin specimens (70°C). The T_g of the unaged resin is 87°C [16]. Dependency of the diffusivity on the immersion temperature is well documented in literature [17] and will not be treated in the present work.

Water uptake was individually tracked for each slice through weight measurements, according to the ASTM D5229/D5229M-14 standard, using a Kern ALJ 160-4NM analytical balance with 0.1 mg resolution. Hourly weighings were performed in the first 8 hours of immersion, two weighings were performed on the second day and the frequency was decreased to one weighing per day for the remainder of the experiment. Only one slice was taken out of immersion at a time, with the complete weighing procedure for each

individual slice taking approximately one minute.

2.3 Diffusivity computation

The experimental water uptake w_{exp} at time t is computed from the measured weight m according to the ASTM D5229/D5229M-14 standard:

$$w_{\mathrm{exp}}(t) = 100 \cdot \left(\frac{m(t) - m_{\mathrm{dry}}}{m_{\mathrm{dry}}} \right) \tag{1}$$

where m_{dry} is the weight measured after the initial drying phase. The diffusion process is considered as one-phase Fickian. Due to the high width/thickness and length/thickness ratios of the slices, the diffusion is modelled as a one-dimensional process in the thickness direction:

$$\frac{\partial c}{\partial t} = D_s \frac{\partial^2 c}{\partial s^2} \tag{2}$$

where $s \in \{x, y, z\}$ is the preferred diffusion direction which depends on the cutting direction of the slice and $c = c(s)$ is the water concentration field. An analytical solution for the volume averaged water uptake during immersion of an initially dry specimen, w_{fick}, can be obtained [13]:

$$w_{\mathrm{fick}}(D_s, w_\infty, t) = w_\infty \left\{ 1 - \frac{8}{\pi^2} \sum_{n=0}^{\infty} \left[\frac{1}{(2n+1)^2} \exp\left(-\frac{D_s (2n+1)^2 \pi^2 t}{h^2} \right) \right] \right\} \tag{3}$$

where w_∞ is the uptake level at saturation and h is the thickness of the slice.

Suitable values for the Fick model parameters D_s and w_∞ have to be chosen in order to fit the experimental uptake points. The fitting procedure can be cast as an unconstrained optimisation problem involving the minimisation of an objective function f which gives the sum of the squared difference between experimental and analytical data:

$$f(D_s, w_\infty) = \sum_t [w_{\mathrm{exp}}(t) - w_{\mathrm{fick}}(D_s, w_\infty, t)]^2 \tag{4}$$

which can be solved for D_s and w_∞.

2.4 Scanning thermal microscopy and local thermal analysis

To study the composite surfaces in search of an interphase region around the fibres, a micro-thermal analyser μTA™ 2990 from TA-Instruments was used. A number of authors conducted studies on the measurement of interphases in thermoset composite materials using μTA [18, 19, 20, 3, 21], showing that micro-thermal analysis may be used to characterize interphases in such composites. The instrument was

calibrated following the procedures described in [22]. Two modes of operation were employed. In a surface mapping mode, the thermal probe was used in AFM-contact mode over a 100μm x 100μm area. The probe was held at a temperature of 60°C (below the glass transition temperature of the epoxy resin). This resulted in images of the topography and of the thermal conductivity. In a second mode, localised thermal analysis (L-TA) was performed. The probe was held in contact at a location selected after the mapping. The temperature of the probe was raised from 25°C to 250°C with a rate of 10 K/s while recording the vertical position of the probe (L-TMA, localised thermomechanical analysis) and the power difference between sample and reference probe needed to realize the programmed temperature ramp (L-CA, localised calorimetry) simultaneously. A measurement in the air was used as a baseline signal.

Glass transition temperatures were evaluated as the onset of the drop in the sensor deflection signal. This corresponds to the beginning of polymer softening. For L-CA measurements, glass transition temperatures are not easily detected for highly crosslinked thermoset materials [20]. After each L-TA measurement, the probe was heated to 600°C over a period of 1 s to remove any residue of polymeric material. The results have been shown to be reproducible.

3 Numerical modelling

3.1 Microscopic diffusion problem

At the macroscopic scale, diffusion is assumed to be orthotropic and can therefore be described by three independent diffusivities D_x, D_y and D_z, with z being the direction parallel to the fibres (Figure 1). It is hypothesised that such orthotropic behaviour is a consequence of the microscopically inhomogeneous nature of the composite material. Therefore, the diffusivity coefficient in each direction can be retrieved through homogenisation of the microscopic diffusion behaviour. Furthermore, it is assumed that the diffusivity coefficient does not depend on time or on water concentration.

At the microscopic scale, the composite material is represented by a three-dimensional RVE composed of unidirectional fibres and surrounding matrix. Since water does not diffuse through the fibres, only the resin is modelled. The fibre arrangements were generated using the discrete element package HADES [23]. A fibre volume fraction of 53.1% was used and the fibre diameter was fixed at 15 μm. A minimum distance of 0.5μm between the fibres was adopted during the contact analysis in order to avoid fibre overlap. The diffusion process is idealised as steady-state [7, 24]:

$$\nabla \cdot \mathbf{j} = 0 \tag{5}$$

where $\mathbf{j}$ is the flux vector. After applying an average (macroscopic) concentration gradient $(\nabla c)^{\mathrm{M}}$ to the

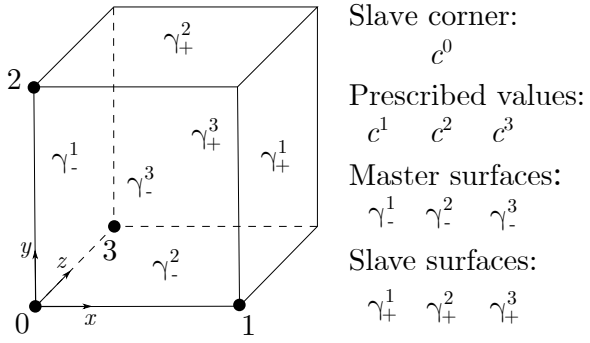

Figure 2: Periodic RVE with prescribed nodes, master and slave surfaces.

RVE, the microscopic water concentration field can be decomposed without loss of generality in:

$$c(\mathbf{x}) = c^0 + (\nabla c)^{\mathrm{M}}\mathbf{x} + \widetilde{c}(\mathbf{x}) \tag{6}$$

where c^0 is the concentration of the origin of the microscopic coordinate frame and $\widetilde{c}$ is a fluctuation field [24].

Consistent homogenisation requires that the volume average of the microscopic concentration gradients must be equal to the applied gradients $(\nabla c)^{\mathrm{M}}$, with the same holding true for the resultant flux $\mathbf{j}^{\mathrm{M}}$:

$$(\nabla c)^{\mathrm{M}} = \frac{1}{|\omega|}\int_{\omega}(\nabla c)d\omega \qquad \mathbf{j}^{\mathrm{M}} = \frac{1}{|\omega|}\int_{\omega}\mathbf{j}\,d\omega \tag{7}$$

with ω being the RVE volume. The use of such homogenisation operators requires the average of gradients and fluxes to be zero at the RVE boundaries [7]. This requirement is enforced by imposing periodicity of concentration at the edges of the micromodel. More details on the homogenization and asymptotic analysis concepts used in the present formulation can be found in [7].

Figure 2 shows the node groups involved in the definition of such periodic boundary conditions. The macroscopic concentration gradient components in the x, y and z directions are applied to the control nodes 1, 2 and 3, respectively:

$$c^s = (\nabla c)^{\mathrm{M}}\mathbf{x}^s \tag{8}$$

where $\mathbf{x}^s$ is a vector with the coordinates of controlling node $s \in \{1, 2, 3\}$. The concentrations on opposing boundary surfaces are then related by:

$$c\big|_{\gamma_+^s} = c\big|_{\gamma_-^s} + c^s \tag{9}$$

In order to ensure that a unique solution exists for the microscopic concentration field, the slave corner node concentration c^0 is adjusted so that the volume average of the concentration is equal to a prescribed value. Recalling that the diffusivity is assumed to be independent of the concentration, an average value of

zero was adopted for convenience.

Finally, the directional macroscopic diffusivity is obtained from the homogenised flux for a unit macroscopic concentration gradient in that direction:

$$D_s = \frac{j_s^{\mathrm{M}}}{(\nabla c)_s^{\mathrm{M}}} = \int_\omega j_s d\omega \tag{10}$$

It is worth mentioning that the concentration gradients and flux components considered in the present formulation are computed only for the resin, since the fibres are not included in the model. The water concentration, gradient and flux for the composite material can be recovered through the relations:

$$c_{\mathrm{comp}} = V_{\mathrm{resin}}\, c_{\mathrm{resin}} \qquad (\nabla c)_{\mathrm{comp}} = V_{\mathrm{resin}}\, (\nabla c)_{\mathrm{resin}} \qquad \mathbf{j}_{\mathrm{comp}} = V_{\mathrm{resin}}\, \mathbf{j}_{\mathrm{resin}} \tag{11}$$

where V_{resin} is the resin volume fraction. It follows that the diffusivity value resulting from integrating only over the resin volume is consistent with the one that would be obtained by also taking the fibre volume into account.

3.2 Interphase modelling

In the preceding formulation, no assumption was made on the diffusivity behaviour of the resin. A simple approach is to consider that the diffusivity of the resin is isotropic, constant at every microscopic point and equal to the one obtained from neat resin immersion experiments. However, literature evidence [3] suggests that diffusion may happen faster in the interphase region close to the fibres [25, 20, 21, 18, 19]. An attempt to experimentally detect the interphase region in the present composite system will be described in Section 4.2.

Joliff *et al*. [3] modelled the interphase as a region with a higher diffusivity than the one of the surrounding bulk resin. Although the authors in [3] considered a constant interphase diffusivity, their own experimental observations suggest that the degree of material modification changes continuously with the distance to the fibre surface. Here, such effect is modelled by using a level set field ϕ to define the distance of any given point to the nearest fibre surface:

$$\phi(\mathbf{x}^{\mathrm{m}}) = \min_{f=1}^{n_{\mathrm{f}}} \left(\sqrt{x\, x_f^{\mathrm{c}} + y\, y_f^{\mathrm{c}}} - r_f \right) \tag{12}$$

where n_{f} is the number of fibres, x^{c} and y^{c} are the coordinates of the fibre centre and r is the radius of the fibre. Since only x and y coordinates are used to compute ϕ, the resultant field is prismatic. The diffusivity

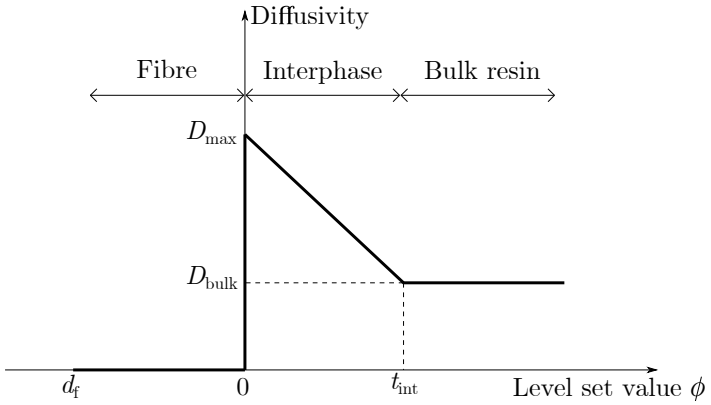

Figure 3: Diffusivity values versus distance to nearest fibre.

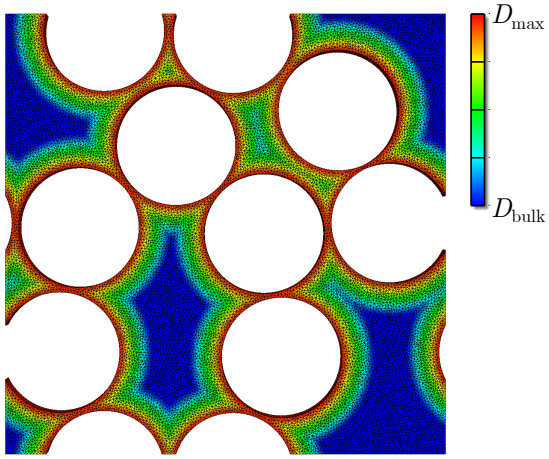

Figure 4: Diffusivity field with an interphase thickness of $4\,\mu$m.

at integration point p is then defined as a linear function of ϕ (Figure 3):

$$D_p = D_{\max} - \phi_p \frac{D_{\max} - D_{\text{bulk}}}{t_{\text{int}}} \tag{13}$$

where $D_{\max}$ and D_{bulk} are the diffusivities at the fibre surface and at the bulk resin, respectively, and t_{int} is the thickness of the interphase region. The choice for a linear function allows for a more realistic representation of the interphase than the one shown in [3] while maintaining the same number of parameters. Figure 4 shows the resultant diffusivity field for an interphase thickness of $4\,\mu$m.

It is important to note that even though diffusivity in pure resin (D_{bulk}) is usually considered isotropic, the same might not hold for the interphase region, for instance due to changes in polymer chain orientation at the immediate vicinity of the fibres [26]. Therefore, no *a priori* assumption will be made regarding the isotropy of $D_{\max}$ in the present study.

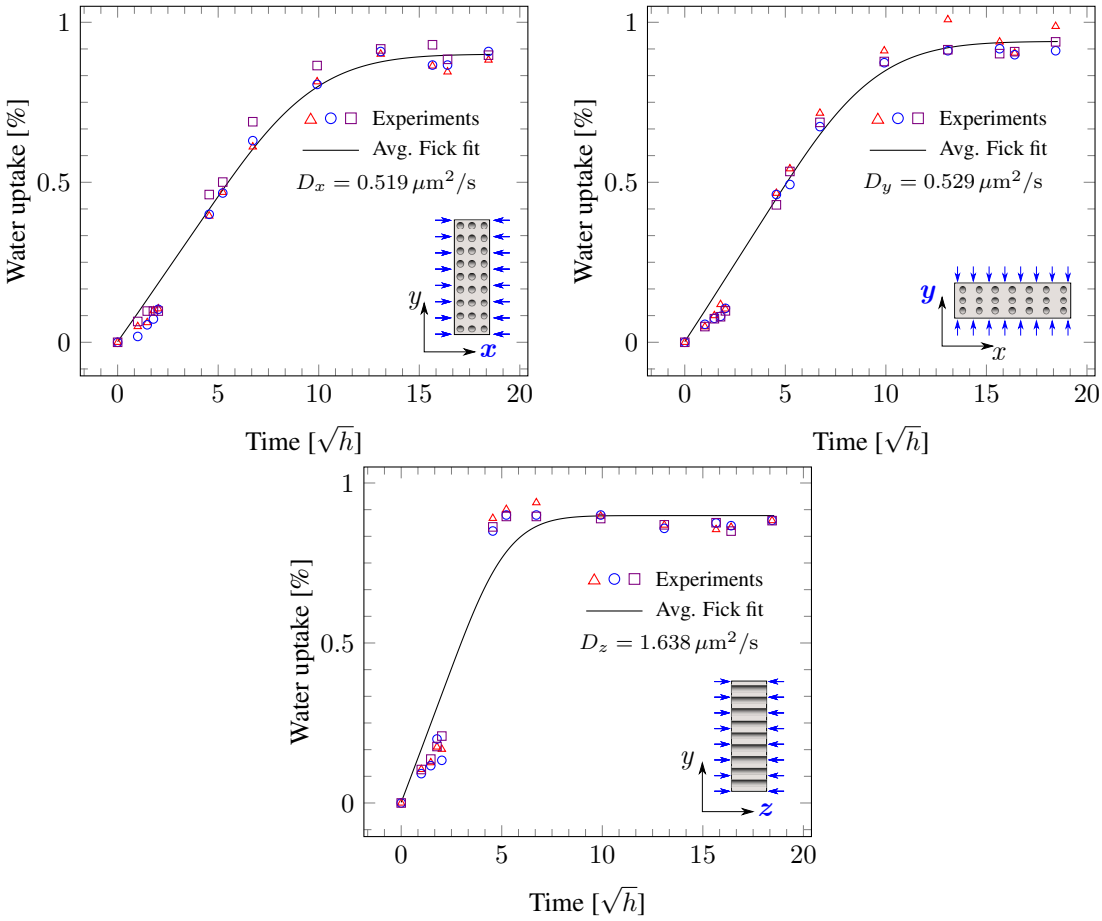

Figure 5: Experimental water uptake results with Fick fit.

4 Results

4.1 Experimental uptake

In Figure 5, experimental water uptake values are plotted for diffusion in each of the x, y and z directions. The represented Fickian diffusion curve for each direction was obtained by fitting the average uptake of 3 specimens using the procedure described in Section 2.3. The final uptake level of approximately 0.91% was similar for all directions.

A Fickian behaviour was observed for all specimen types, although small deviations are observed for diffusion along the z direction between 20 h and 50 h of immersion. The diffusivities obtained for the x and y directions of approximately 0.52 $\mu\text{m}^2/\text{s}$ were similar, which was expected due to the similar fibre arrangement inside the samples. For these two directions, saturation was reached after approximately 300 h of conditioning. On the other hand, a diffusivity of 1.638 $\mu\text{m}^2/\text{s}$ was obtained for diffusion in the z direction, approximately 3 times higher than in the other directions. In this case, saturation was reached after approximately 100 h of immersion.

The observed anisotropy in diffusivity was expected and also observed by other authors [13, 9]. This effect is usually attributed to the fact that the fibres act as barriers to the water movement in the x and y directions, whereas diffusion in the z direction runs along the fibres and is therefore unhindered. For the present epoxy system, the diffusivity in pure resin specimens is 0.741 $\mu\mathrm{m}^2/\mathrm{s}$ [16]. As expected, diffusivities in the x and y directions are lower than the pure resin one due to the aforementioned barrier effect. For the z direction, however, a value approximately twice as high as for pure resin is obtained. It is clear that the barrier effect caused by the fibres is not enough to fully explain the anisotropic diffusion behaviour observed for this material system as it cannot explain such increase in diffusivity in the z direction.

4.2 Interphase measurement

In Figure 6, the thermal conductivity map obtained with micro-thermal analysis is shown, clearly displaying the contrasts between fibres and the surrounding epoxy resin. In such conductivity mapping, the fibres are observed as zones with a higher power value, since the bulk thermal conductivity for the glass is about four times higher than the value for epoxy resin. As the probe moves away from a fibre, the thermal conductivity decreases gradually to a lower level corresponding to the resin. To determine the width of the interphase in the thermal map, line scans drawn in several directions across the detected glass fibres show a transition zone which extends over 4-5 μm (Figure 7).

To determine the origin of this thermal conductivity gradient, L-TMA measurements were made in positions with different (increasing) distances from the centre of the fibre (Figure 8). In the bulk of the material, sufficiently far from the fibres, the glass transition temperature is constant. As the distance to the fibre decreases, the glass transition temperature decreases by 10-15 K in an interphase region of 4-5μm (Figure 9) and may be defined as the area where the softening temperature is lower than the softening temperature of the bulk. The distance over which this decreasing T_g stretches is comparable to the distance over which the gradual evolution in thermal conductivity is observed in the surface mapping (Figure 6). The L-TMA curve measured on the fibre shows only thermal expansion. The presence of an interphase may be attributed to incomplete curing or modification of the bulk resin after chemical reactions with the sizing applied to the fibres, also seen for instance by Mallarino *et al.* [21].

In a similar study performed by Joliff *et al.* [3], the authors measured interphase thickness values using both micro-thermal analysis and atomic force microscopy (AFM), with values ranging from 1 μm obtained through AFM force measurements to 4 μm of highly modified resin and 6 μm of slightly modified resin obtained through local T_g measurements. Since significantly different values are obtained for the same material system by using different techniques, the models of the next sections will consider both a thin interphase of 1 μm and a thick interphase of 4 μm.

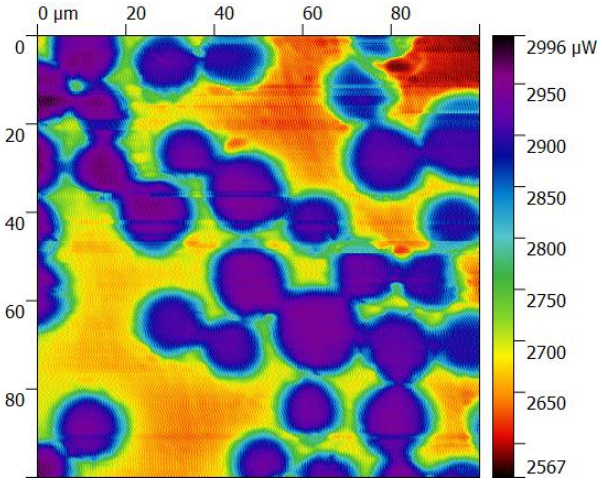

Figure 6: Thermal conductivity profile in a 0.01mm^2 area of a z-direction slice.

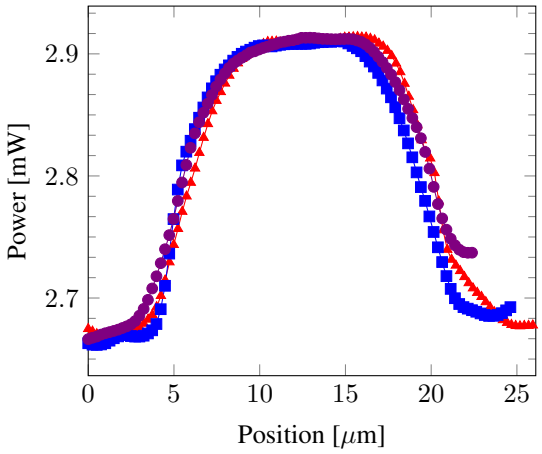

Figure 7: Three different line scans of thermal conductivity in the vicinity of a fibre.

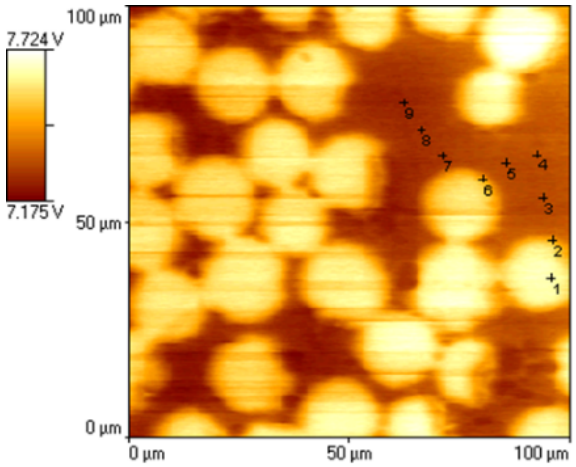

Figure 8: Surface map obtained through μTA in a 0.01mm^2 area of a z-direction slice showing L-TMA test locations.

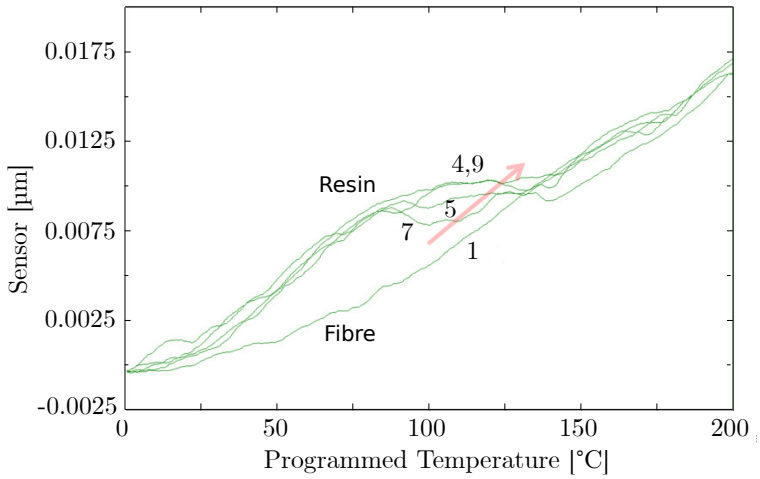

Figure 9: L-TMA experiments at increasingly distant locations from a glass fibre.

4.3 RVE study

The anisotropic diffusivity behaviour of the present material system was obtained through homogenisation of the response of a Representative Volume Element (RVE) according to the formulation presented in Section 3. This section describes the parametric study performed in order to chose a representative micromodel for comparison with the experimental behaviour.

In order to correctly represent the diffusivity behaviour of the interphase region, particularly where the distance between fibres is small, an adequate mesh density is required. Figures 10 and 11 show the obtained diffusivity values in the x and z directions for 50 different 5 x 5 fibre micromodels (90 μm x 90 μm) with varying characteristic element size ranging from 3 μm to 0.3 μm in steps of 0.05 μm. In all cases, the discretisation in the z direction consisted of a single layer of elements, which is sufficient to solve the steady state flow in that direction exactly for the given prismatic geometry. For the parametric study, $D_{\max}$ was considered isotropic and a ratio $D_{\max}/D_{\text{bulk}}$ of 10 was adopted in order to investigate the relative differences between models with thin and thick interphases. Choosing an appropriate ratio is not crucial at this point since only relative differences between the two interphase thicknesses are of interest for the parametric study. Wedge elements with three integration points were used.

As expected, the diffusivities converge to stable values as the mesh density increases. For both directions and interphase thicknesses, such stabilisation happened at an element length of approximately 0.5 μm. For both directions, the final diffusivities for the thick interphase models showed significantly higher scatter than the thin interphase ones. It is possible that this behaviour is induced by the larger area of influence of fibres with thick interphases. The interphases of adjacent fibres tend to overlap more often and the resultant interaction between fibres makes the thick interphase model more sensitive to changes in fibre arrangement.

With a fixed element length of 0.5 μm, the next calibration step involved choosing an RVE size large

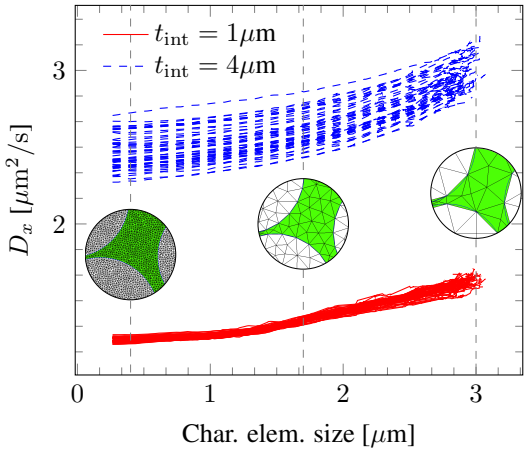

Figure 10: Changes in diffusivity of 50 different micromodels with increasing mesh density (x direction).

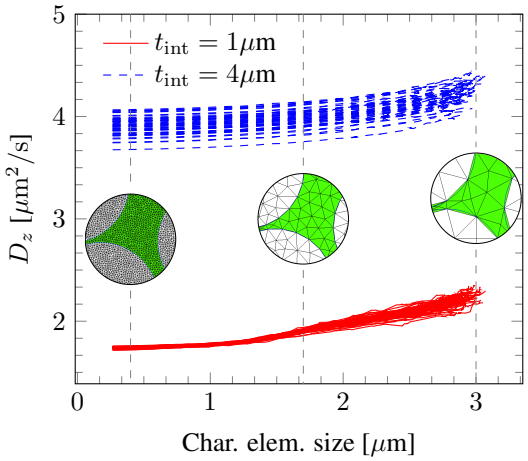

Figure 11: Changes in diffusivity of 50 different micromodels with increasing mesh density (z direction).

enough to ensure that the resultant homogenised diffusivity does not change considerably if the size is further increased. Figures 12 and 13 show homogenised diffusivity values in the x and z directions for both thin and thick interphase thicknesses with increasing RVE size, expressed by its number of fibres (from 1 x 1 to 9 x 9 fibres). The plotted values represent average values from 50 different micromodels and the bars represent standard deviations.

Consistent with the results obtained for 5 x 5 micromodels, the response of models with a thick interphase had a higher scatter when compared to models with a thin interphase. Nevertheless, the average response of both types of model reached a stable value from a 3 x 3 RVE size. For the final comparison with experimental results, an RVE size of 5 x 5 fibres was chosen as a compromise between precision and computational effort.

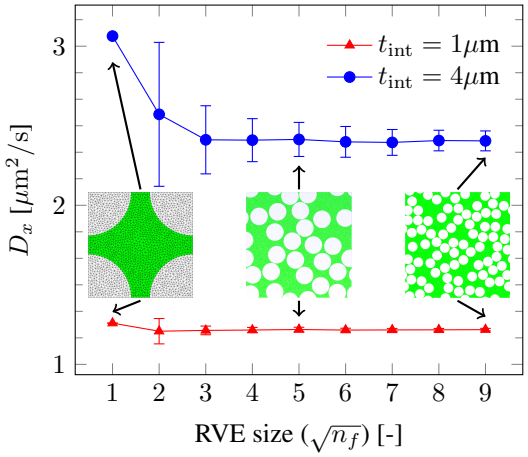

Figure 12: Effect of RVE size on the obtained diffusivities (x direction).

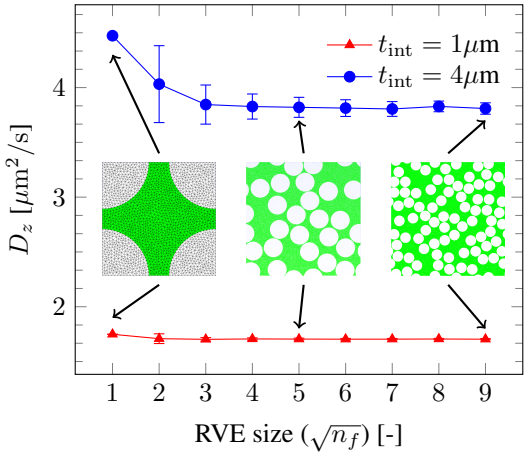

Figure 13: Effect of RVE size on the obtained diffusivities (z direction).

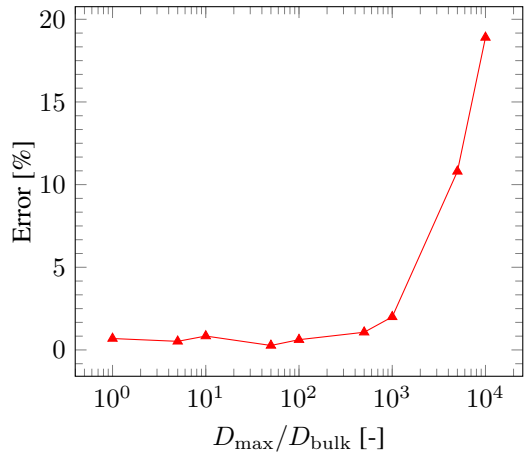

Figure 14: Steady-state model error.

4.4 Validation of the steady state assumption

For high $D_{\max}/D_{\text{bulk}}$ ratios, flow in the z direction mostly takes place through the interphases. In the limit case, the interphases are instantly saturated along the whole thickness of the specimen, with subsequent diffusion happening radially from the fibres into the surrounding resin in the x and y directions. In such case, the assumption of steady-state flow in the z direction is invalid and a full microscale transient analysis becomes necessary to capture the physics of water uptake in slices that are thin in the z direction.

In order to validate the steady state assumption, transient analyses were also performed to simulate the uptake in the z direction. For these simulations, the micromodel was extruded to match the actual thickness of the slice. The same fitting procedure as for the experimental results was used to obtain an effective diffusivity parameter from the transient analysis results.

Figure 14 shows the error $(D_{\text{trans}} - D_{\text{steady}})/D_{\text{trans}}$ in the diffusivity obtained with the steady-state micromodel with respect to the one obtained from the transient analysis. For ratios of up to 500 between the interphase and bulk diffusivities, the steady-state assumption led to errors smaller than 1%. Further increasing the ratio causes the error to increase, with up to 20% difference observed for $D_{\max}/D_{\text{bulk}} = 10000$. Since such high ratios are not realistic, the steady-state assumption is valid for obtaining the diffusivity in all three directions.

4.5 Numerical results and discussion

The proposed RVE diffusion model was used in an attempt to reproduce the obtained experimental results. A 5 x 5 fibre RVE size was adopted and the results were computed as an average of 50 executions with different RVE geometries since scatter is still present for such size. The characteristic element size was fixed at 0.5 μm in the x-y plane, with a single layer of elements in the z direction. The resultant diffusivities for all models are shown in Table 1 and the resultant uptake curves can be seen in Figure 15.

	D_{bulk}	$\left(\frac{D_{\max}}{D_{\text{bulk}}}\right)_{x,y}$	$\left(\frac{D_{\max}}{D_{\text{bulk}}}\right)_{z}$	t_{int}	D_x	D_y	D_z
	[μm^2/s]	[-]	[-]	[μm]	[μm^2/s]	[μm^2/s]	[μm^2/s]
Experimental	-	-	-	-	**0.519**	**0.529**	**1.638**
No interphase	0.741	-	-	-	**0.397**	**0.389**	**0.741**
Thick int. [3]	0.741	5.0	5.0	4.0	**1.368**	**1.353**	**2.149**
Thin int. [3]	0.741	5.0	5.0	1.0	**0.832**	**0.826**	**1.187**
Thick int. fit	0.741	1.5	1.5	4.0	**0.538**	**0.529**	**0.928**
Thin int. fit	0.741	2.1	2.1	1.0	**0.537**	**0.529**	**0.863**
Anisotropic fit	0.741	1.5	3.5	4.0	**0.538**	**0.529**	**1.638**

Table 1: Comparison between experiments and numerical simulations.

For the first model (*no interphase*), the level set field was not used and the diffusivity of every material point was equal to D_{bulk}. Therefore, only the effect of geometric inhomogeneity was taken into account in this case. As expected, the homogenised diffusivities in the x and y directions were lower than the neat resin one, due to the barrier effect caused by the fibres. In the z direction, since no obstacles are present, the obtained diffusivity is equal to D_{bulk}. Compared with the experimental results, the values provided by the model are approximately 27% lower for D_x and D_y and 55% lower for D_z, suggesting the presence of additional mechanisms that accelerate the diffusion process.

For the next two models (*thick int.*, *thin int.*), the level set field was used to allow for higher diffusivity at the interphase regions and the ratio $D_{\mathrm{max}}/D_{\mathrm{bulk}} = 5$ proposed by Joliff *et al.* [3] was adopted. For these models, isotropic diffusivity was assumed at the interphase. As expected, the inclusion of an interphase yields higher homogenised diffusivity values. For both cases, however, the resultant values for D_x and D_y were higher than the experimental ones. The $D_{\mathrm{max}}/D_{\mathrm{bulk}}$ ratio proposed in [3] is therefore not valid for the present material system.

Since the diffusivity ratio proposed by Joliff *et al.* [3] was not based on a direct measurement, only the values for t_{int} were kept for the next two models (*thick int. fit*, *thin int. fit*) and D_{max} was adjusted in order to fit the experimental value for D_y. For a thick interphase, the obtained ratio between D_{max} and D_{bulk} was 1.5, while a ratio of 2.1 was found for a thin interphase. Even though both models correctly capture the diffusion mechanics in the x-y plane, the diffusivity along the fibres was still approximately 43% lower than the one obtained from the experiments.

The results indicate that the combination of geometric inhomogeneity and linearly increasing diffusivity at the interphase is not enough to explain the experimental value for D_z. We see three different potential explanations for this effect. Firstly, polymer chain orientation close to the fibre/matrix interface is unlikely to be isotropic [27, 26], which could give rise to anisotropic water diffusivity. Secondly, water movement through capillarity in micro cracks would be significantly faster than diffusion in bulk resin [28, 6]. These cracks are caused by fibre/matrix debonding and are therefore oriented parallel to the fibres. It is reasonable to suppose that such cracks would accelerate diffusion the most in the fibre direction. Thirdly, z direction slices are more delicate and therefore more susceptible to manufacturing damage. If the two first explanations are dominant, they can be represented in a homogenised sense by assuming anisotropic diffusion in the interphase, similar to the approach proposed in [6]. To demonstrate this, a fit for all directions can be obtained by relaxing the assumption of isotropic diffusion at the interphase (*anisotropic fit*). Keeping the hypothesis of a thick interphase, a ratio $\left(D_{\mathrm{max}}/D_{\mathrm{bulk}}\right)_z$ of 3.5 was found to give an optimal fit for the uptake in the z direction. It is important to note that since another fit parameter was added, no unique solution exists for this case and a similar fit could be obtained with a thin interphase.

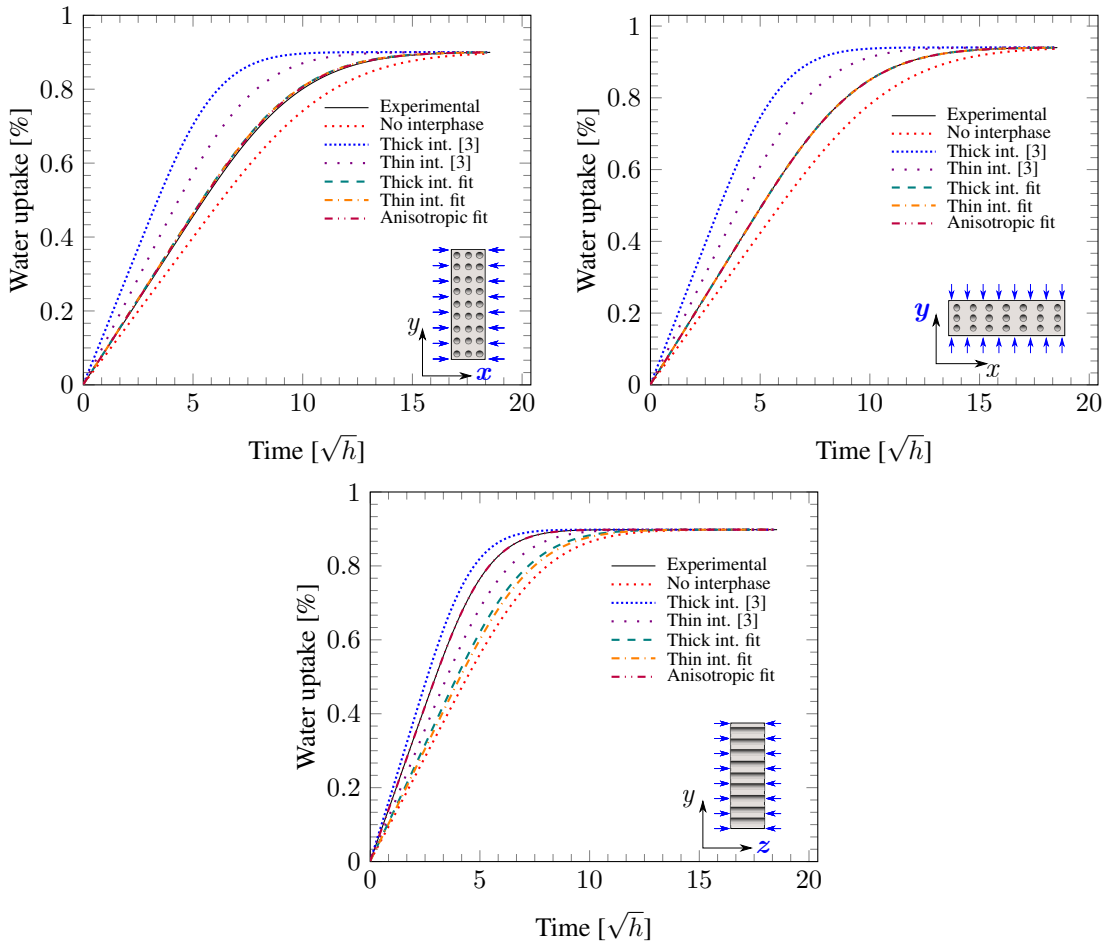

Figure 15: Numerical water uptake results.

5 Conclusions

In this work, a combined numerical and experimental investigation of the anisotropic water diffusion behaviour of unidirectional glass/epoxy composites has been performed. The experimental procedure consisted of manufacturing a thick unidirectional panel from which material slices were cut in each of the orthotropy planes of the material and immersed in water at 50°C. The experimental diffusivities were obtained by fitting an analytical Fick solution to the uptake results. Furthermore, a measure of the interphase thickness in the vicinity of the fibres was performed through micro-thermal analysis. In order to gain further insight in such anisotropic water movement, the diffusion process was modelled in a three-dimensional RVE from which homogenised diffusivity values were obtained. A level set field was used to retrieve the distance of any resin point to the nearest fibre and allow for faster diffusion in the interphase region.

From the experimental results, a similar uptake behaviour was observed for diffusion in directions transverse to the fibres due to a comparable fibre arrangement, with saturation being attained after approximately 300 hours of immersion. On the other hand, diffusion in the longitudinal direction was significantly faster

and a saturated state was reached after approximately 100 hours. Even though the diffusivities in the transverse directions followed the expected trend of being lower than the neat resin one due to a barrier effect caused by the fibres, the diffusivity along the fibres was found to be twice as high as the neat resin one, a fact that cannot be explained by the barrier effect alone. From thermal analysis, an interphase region of softer resin with a thickness of 4-5 μm was detected, suggesting that diffusion may happen at a faster rate close to the fibres.

For the numerical investigation, a parametric study was performed on the RVE size and finite element mesh density. For comparison with the experimental diffusivities, a characteristic element size of 0.5 μm was chosen and the homogenised diffusivities were obtained as the average result of 50 realisations with different fibre arrangements. Results showed that the geometric effect of fibres acting as barriers for the water movement is indeed responsible for part of the observed anisotropy. However, it was not possible to fit the experimental values by using only the bulk epoxy diffusivity. With the addition of an interphase around the fibres, a fit could be obtained for diffusion in both transverse directions, although the diffusivity ratios proposed in [3] were not valid for the present material system. Nevertheless, the combination of the aforementioned barrier effect and faster isotropic diffusion at the interphase was not sufficient to be able to fit experimental results in all three directions with a single set of parameters. Such a fit could only be found by making the interphase diffusivity orthotropic with a higher value in the direction parallel to the fibres.

Acknowledgements

The authors acknowledge the contribution of the TKI-WoZ and IRPWIND projects for motivating and partly funding this research and of the TKI-MIMIC project industrial partners for providing useful feedback.

References

[1] Y. Hu, A. W. Lang, X. Li, S. R. Nutt, Hygrothermal aging effects on fatigue of glass fibre/polydicyclopentadiene composites, Polym Degrad Stabil 110 (2014) 464–472.

[2] L. Gautier, B. Mortaigne, B. V., Interface damage study of hydrothermally aged glass-fibre-reinforced polyester composites, Compos Sci Technol 59 (1999) 2329–2337.

[3] Y. Joliff, W. Rekik, L. Belec, J. F. Chailan, Study of the moisture/stress effects on glass fibre/epoxy composite and the impact of the interphase area, Compos Struct 108 (2014) 876–885.

[4] F. Naya, C. González, C. S. Lopes, S. van der Veen, F. Pons, Computational micromechanics of the transverse and shear behaviour of unidirectional fiber reinforced polymers including environmental effects, Compos Part A-Appl S 92 (2017) 146–157.

[5] Y. J. Weitsman, Coupled damage and moisture-transport in fiber-reinforced, polymeric composites, Int J Solids Struct 23 (1987) 1003–1025.

[6] Y. J. Weitsman, Anomalous fluid sorption in polymeric composites and its relation to fluid-induced damage, Compos Part A-Appl S 37 (2006) 617–623.

[7] I. Özdemir, W. A. M. Brekelmans, M. G. D. Geers, Computational homogenization for heat conduction in heterogeneous solids, Int J Numer Meth Eng 73 (2008) 185–204.

[8] A. R. Melro, P. P. Camanho, F. M. Andrade Pires, S. T. Pinho, Micromechanical analysis of polymer composites reinforced by unidirectional fibres: Part I - Constitutive modelling, Int J Solids Struct 50 (2013) 1897–1905.

[9] H. S. Choi, K. J. Ahn, J. D. Nam, H. J. Chun, Hygroscopic aspects of epoxy/carbon fiber composite laminates in aircraft environments, Compos Part A-Appl S 32 (2001) 709–720.

[10] I. B. C. M. Rocha, S. Raijmaekers, R. P. L. Nijssen, F. P. van der Meer, L. J. Sluys, Experimental/numerical study of anisotropic water diffusion in glass/epoxy composites, IOP Conf Ser: Mater Sci Eng 139 (2016) 1–8.

[11] Technical data sheet - EPIKOTE resin MGS RIMR 135 and EPIKURE curing agent MGS RIMH 134-RIMH 137, Tech. rep., Momentive (2006).

[12] Technical data sheet - PPG fiber glass: Hybon 2002 roving, Tech. rep., PPG (2010).

[13] S. A. Grammatikos, B. Zafari, M. C. Evernden, J. T. Mottram, J. M. Mitchels, Moisture uptake characteristics of a pultruded fibre reinforced polymer flat sheet subjected to hot/wet aging, Polym Degrad Stabil 121 (2015) 407–419.

[14] G. M. Odegard, A. Bandyopadhyay, Physical aging of epoxy polymers and their composites, J Polym Sci Pol Phys 49 (2011) 1695–1716.

[15] T. C. Wong, L. J. Broutman, Water in epoxy resins part II. diffusion mechanism, Polym Eng Sci 25 (1985) 529–534.

[16] I. B. C. M. Rocha, S. Raijmaekers, R. P. L. Nijssen, F. P. van der Meer, L. J. Sluys, Hygrothermal ageing behaviour of a glass/epoxy composite used in wind turbine blades, Compos Struct 174 (2017) 110–122.

[17] B. Dewimille, A. R. Bunsell, Accelerated ageing of a glass fibre-reinforced epoxy resin in water, Composites 14 (1983) 35–40.

[18] R. Häßler, E. Mühlen, An introduction to μta(tm) and its application to the study of interfaces 361 (2000) 113–120.

[19] G. Van Assche, B. Van Mele, Interphase formation in model composites studied by micro-thermal analysis, Polymer 43 (2002) 4605–4610.

[20] M. S. Tillman, B. S. Hayes, J. C. Seferis, Examination of interphase thermal property variance in glass

fiber composites 392-393 (2002) 299–302.

[21] S. Mallarino, J. F. Chailan, J. L. Vernet, Interphase investigation in glass fibre composites by micro-thermal analysis, Compos Part A-Appl S 36 (2005) 1300–1306.

[22] H. R. Fischer, Calibration of micro-thermal analysis for the detection of glass transition temperatures and melting points - repeatability and reproducibility 92 (2008) 625–630.

[23] F. P. van der Meer, Micromechanical validation of a mesomodel for plasticity in composites, Eur J Mech A-Solid 60 (2016) 58–69.

[24] K. Terada, M. Kurumatani, Two-scale diffusion-deformation coupling model for material deterioration involving micro-crack propagation, Int J Numer Meth Eng 83 (2010) 426–451.

[25] J. Kim, M. Sham, J. Wu, Nanoscale characterisation of interphase in silane treated glass fibre composites, Compos Part A-Appl S 38 (2001) 607–618.

[26] L. S. Faraji, Nanoscale carbon fiber-matrix interphase characterization with atomic force microscopy indentation, PhD thesis, Oklahoma State University, 2014.

[27] M. Malagù, A. Lyulin, E. Benvenuti, A. Simone, A molecular-dynamics study of size and chirality effects on glass-transition temperature and ordering in carbon nanotube-polymer composites, Macromol Theory Simul 25 (2016) 571–581.

[28] P. Davies, F. Pomies, L. A. Carlsson, Influence of water and accelerated aging on the shear fracture properties of glass/epoxy composite, Appl Compos Mater 3 (1996) 71–87.